Instrument Science Report WFC3 2020-05

WFC3 IR sensitivity over Time

V. Kozhurina-Platais, S. Baggett

April 17, 2020

Abstract

The observations of the globular cluster ω Cen taken with the Wide Field Camera 3 Infrared Detector (WFC3/IR) in F160W filter over more than 10 years have been used to examine the secular changes in the detector's sensitivity and search for its variations with time. The WFC3/IR sensitivity appears to be changing at the level of 0.2% (0.002 mag) per year. There is also possibility of the abrupt changes in the WFC3/IR sensitivity around mid-2011. In addition to the secular changes, there is significant scatter in the sensitivity variations at the $\pm$2% level during each interval of the orbital target visibility, which is consistent with the effect of orbital breathing.

1. Introduction

The Wide Field Camera 3 infrared channel (WFC3/IR) on the Hubble Space Telescope (HST) provides high-resolution, relatively low noise IR imaging capability, spanning 800 - 1700 nm. With a 136" x 123" field of view (0.13 "/pix), the camera is designed to reach the limiting magnitude of 29 AB mag in 10 hours (Dressel,*et al* 2019). The 15 filters (wide, medium, and narrow passbands) and two grism filters on WFC3/IR enable a variety of science projects such as stellar populations and its physics, star formation, cosmology, exoplanets, solar system planets, and much more. Therefore, quantifying the stability of the detector's sensitivity and assessing potential systematic uncertainties is of paramount importance.

The photometric calibration programs for WFC3/IR over the past ten years have employed primarily spectrophotometric standard stars to monitor the IR channel throughput and set the absolute photometric zero points. The IR aperture photometry in various passbands filters has been relatively stable, although showing a short-term 1-sigma repeat-ability of ±1.5% (Baja, 2019). The photometric scatter has been reduced to ±0.5% when dither steps of at least 10 pixels are used in the observations. Despite the 10-year baseline, the significant short-term scatter in the standard star observations prevents the detection of subtle long-term trends seen in Bajaj (2019, Figure 7).

The authors of a recent study of WFC3 grism data binned the standard star spectra over the bulk of each grisms throughput range, thereby boosting the signal to noise (S/N) and revealing small long-term declines in sensitivity: 0.169%±0.015% per year for G102 and 0.085% ±0.014% for G141. The RMS scatter (1-sigma broadband uncertainty of a single observation) is ∼0.45% and 0.42% for the G102 and G141, respectively (Bohlin & Deustua, 2019). Motivated by this evidence of a secular trend, we re-purposed archival observations of the stellar cluster ω *Cen* originally taken for astrometric calibrations (e.g. for obtaining distortion solutions, monitoring the plate-scale over time) to evaluate whether a change in sensitivity is discernible in a wide passband filter, or whether the long-term effects are limited to the grisms only. The astrometric calibration data are acquired at a relatively frequent cadence, targeting a globular cluster with a large number of stars, so that the photometric errors are simultaneously reduced compared to a single star, thus improving the ability to measure small changes in the IR sensitivity. This report presents the data used, describes the PSF-fitting method applied to obtain the photometry, and quantifies the detected trends.

2. HST/WFC3 IR

2.1. Observations and Reductions

The globular cluster ω *Cen* is the target in multi-cycle calibration programs over the last 11 years of WFC3 on HST. All observations of ω *Cen* taken through the F606W and F160W UVIS and IR filters respectively, (a total of 32 and 26 epochs) were used to: 1) derive the skew of the geometric distortion and look for any secular changes over time and/or during the orbital time of target visibility; 2) monitor the optical and mechanical stability of the WFC3/UVIS and IR, using a single filter in each channel; 3) keep a continuous record of the WFC3 stability and/or any time-dependency. These multiple cycle UVIS and IR observations are characterized by a wide range of offsets (POSTARG) and orientations.

Figure 1 shows the footprint of all F160W IR filter observations in the core of globular cluster ω *Cen* over ∼10 years. ω *Cen* is the largest and the most massive globular cluster in the Milky Way with gradually and moderately increasing spatial density toward its center.

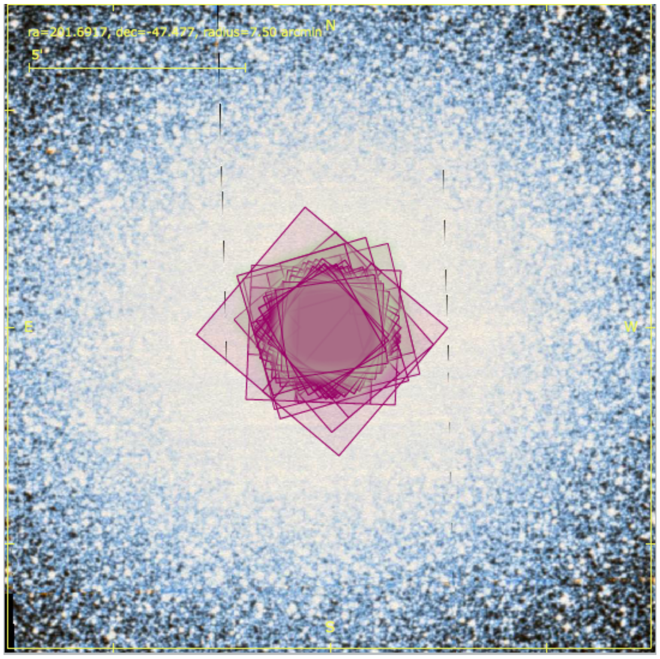

Fig. 1.— Footprint of WFC3/IR observations in the center of globular cluster ω *Cen*.

The core radius of the cluster $\sim 2\farcm37$ (Harris, 1996) is similar to the size of the field-of-view of the WFC3/IR images ($2\farcm05 \times 2\farcm26$). Since all ω *Cen* observations were taken near the center of the cluster, there is a weak density change along the radial direction of the density profile in any of our IR images and thus there is no strong evidence of the stellar radial density profile. As seen in Fig.2 (Kozhurina-Platais & Anderson, 2015), the stars exhibit a nearly flat distribution, indicating a homogeneous star list from very heterogeneous data.

The first step in the analysis of stellar images taken with WFC3/IR is to measure any changes in the response of an imaging system to a point source i.e. point-spread function (PSF). The quality of the PSF is characterized by its shape, position and the flux at the time of observation. An accurate X&Y positions and flux can be measured with accurate PSF model, if the PSF itself is broad enough, i.e. that flux is spread over a few pixels. The WFC3/IR PSF is known to be severely under-sampled, the FWHM $\simeq$1.3 pixels, which means more than 1/2 of the flux is contained within the central IR pixels. The variations of PSF across the IR detector is another complication for accurate measurements of X&Y positions and the flux. Thus, the accuracy of the sensitivity measurements depends on the accuracy of the measured stellar fluxes and X&Y positions on the images using by accurate PSF model. Initially, Anderson & King (2000) developed a purely empirical model (in their notation, *effective* PSF or ePSF) to describe the WFPC2 PSF and provide high-precision photometry and astrometry from WFPC2 images. In 2006, they extended this model to the ACS/WFC (Anderson & King 2006) and represented its spatial variations by an array of 9×5 fiducial PSFs across each ACS/WFC CCD chip. A similar treatment was used for WFC3/UVIS, an array of 7×4 PSFs across each WFC3/UVIS chip. Analogous to ACS/WFC and WFC3/UVIS, the PSF construction has been applied to the WFC3/IR PSF (Anderson, 2016) using an array of 3×3 PSF across the IR detector[1]. The FORTRAN software *hst1pass.F* (the newly updated version for all HST imaging detectors, Anderson private communication) uses these ePSF models to find and measure the stars in the WFC3/IR images. The parameters were set to identify every pixel that had no brighter pixels within a radius of one IR pixels and was brighter than sky background by 0.5e^-/sec within its central 2×2 pixels to qualify as potential star. The parameter of the perturbation to the IR PSF is not use since an array 3×3 PSF across the IR detector is not enough to measure a global perturbation to the PSF as in the case ACS/WFC and WFC3/UVIS. The central 5×5 pixels were then fit with the local PSF to determine a position and flux. The output from this routine is a list of high-precision X&Y raw positions, the distortion–corrected X&Y positions (accurate to the level of 0.01 pixel), flux and the QU quality parameter of PSF fit (derived using the residuals to the PSF fit) for each star. On average a total of $\sim$ 6500 stars were measured in each of the IR-image. This is a sufficient number of stars to look with confidence for systematic trends in the WFC3/IR X&Y and flux measurements. Figure 2 shows typical instrumental IR magnitudes ($Inst.mags = -2.5log(\frac{Flux}{Exp.Time}$) versus the quality parameter QU. The stars brighter than -12.5 instrumental magnitude are saturated and the quality of the PSF fit becomes poor. For well–measured stars within the range of $-12.5 \lesssim$ Inst.mag. $\lesssim -10$, the QU of a PSF fit is less than 0.05.

[1]http://www.stsci.edu/hst/instrumentation/wfc3/data-analysis/psf

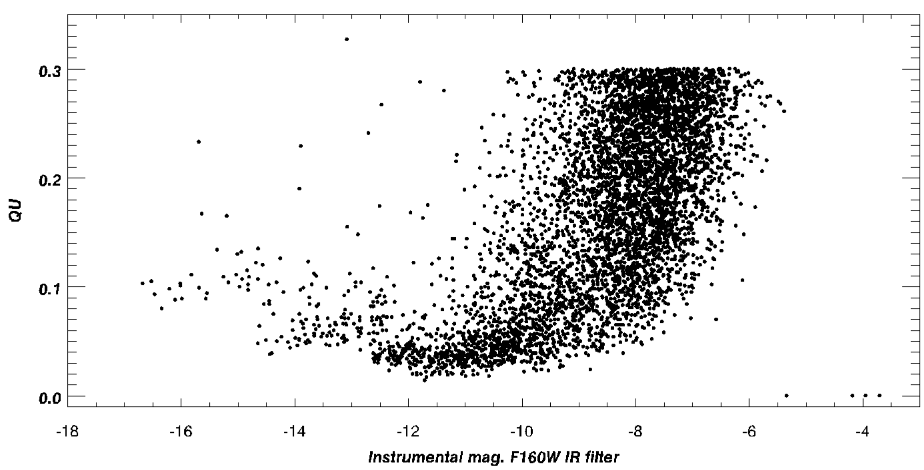

Fig. 2.— Quality parameters of PSF fit (QU) as a function of instrumental magnitude for all stars found in a typical IR F160W image. The stars brighter than about $\lesssim -12.5$ instrumental magnitude are saturated. Star with instrumental magnitude $-12.5 \lesssim$ Inst.mag. $\lesssim -10$, are well–measured and the QU of fit is less than 0.05. The stars with instrumental magnitude $\gtrsim -10$ are fainter stars with low S/N and are not well measured.

2.2. Matching the stars: Astrometric and Photometric

To compare the photometry for all stars common to all observations a 6-parameter linear transformation was used to match their X&Y positions. This is a standard astrometric technique which allows one to match with high precision X&Y positions between each exposure and the reference frame and simultaneously retain the photometric information for each star in common:

$$X_i^1 = A + B\times X_i + C\times Y_i \quad (1)$$
$$Y_i^1 = D + E\times X_i + F\times Y_i \quad (2)$$

where X_i^1, Y_i^1 are positions in the first IR ω *Cen* observation selected as a reference frame , and X_i,Y_i are positions corrected for distortion for each star from each subsequent IR exposure; A, D are offsets between the two coordinates systems; B,C,E,F are linear terms. A least-squares method was used to solve for these 6 parameters. Each solutions was based on 2000 to 5000 common between exposure and the reference frame. This a sufficient number of stars to look for any astrometric systematic errors as well for any residuals in the photometric information for common stars. The RMS of all solutions is 0.02 - 0.08 IR pixels (or 7 mas on the sky).

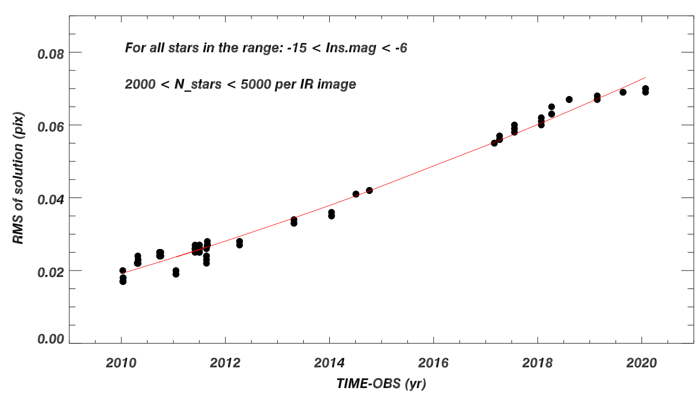

Fig. 3.— *RMS* of the linear solution as a function of time for each IR image of ω *Cen* taken through F160W filter. The Y-axis is in IR pixels (one pixel is $\sim 0\overset{''}{.}13$).

Figure 3 shows the RMS of each solution as function of time. As seen in Figure 3, the RMS of solution appears to be gradually changing with time from the minimum ∼0.02 IR pixel (in year ∼ 2010) to the maximum of ∼0.07 IR pixel (in year ∼ 2020). In fact, this trend in the *RMS* of solutions is an indication of the internal motions of stars in ω *Cen*. As reported by Anderson & van der Marel (2010), the internal velocity dispersion in the proper motions of ω *Cen* is at the level of 0.9 *mas* per year. The epoch difference between the first and the last WFC3/IR observations of ω *Cen* is $\sim$11 years, which contributes as much as $\sim$0.076 IR pixel drift in the RMS of the solutions.

Once we have validated the accurate astrometric linear transformations of X&Y positions of common stars between the chosen initial WFC3/IR observation and each following IR observation of ω *Cen*, we proceed to the comparison of the photometry of these stars over time.

3. Photometric Trend

From the astrometric transformations described in Sect.2.2, the photometric offsets between common stars of the first reference image ($Ins.Mag_o$) with the next one ($Ins.Mag_i$) were averaged as follows $D(mag) = \frac{\sum_{i=1}^{N}(Ins.Mag_i - Ins.Mag_o)}{N}$, where N is the number of common stars between two WFC3/IR images. The standard error of the mean is calculated for each individual offset. Figure 4 shows the calculated photometric offsets as a function of time with over-plotted standard errors.

As can be seen in Figure 4, it appears that the photometric offsets are changing with time. In order to quantify the potential variation of the IR flux over time, a linear fit $f(D(mag)) = a + b \times T$ is used, where argument T is the time of observation. The slope of this fit, coefficient b, is equal to -0.0027$\pm$0.0004, and it is statistically significant at the 7σ level. Figure 4 also shows a significant scatter in the distribution of photometric offsets between 2010 and 2011 (Modified Julian Date $\sim$ 55175-55800), two years after Servicing Mission 4 in May 2009. During that period of time there are many observations from programs for astrometric and as well photometric calibrations of the IR detector. These observations were taken with POSTARGs (slightly shifting the telescope in *RA* and *Dec* directions at about $\pm 30''$) during several consecutive HST orbits (CAL-11928, CAL-12094 etc). Figure 5 shows the photometric offset versus time for a period of one year, in the range of Modified Julian Date $\sim$ 55175-55800 (December 2009 - August 2010).

As can be seen in Figure 5, around MJD $\sim$55178 (December 2009) over very short period of time when the observations were taken during several sequential HST orbits, the total amount of photometric offset ranges from -0.02 to $+0.02$. Similarly, at MJD $\sim$55275 (March 20, 2010) the averaged offset is in the range from -0.02 to $+0.02$. As shown in Kozhurina-Platais *et al* (2012), the astrometric scale over this time span changes during the orbital target visibility and a jumps with each re-acquisition of guide stars. The observed variations of skew are also related to the orbital events such as the target occultation and the orbital target visibility, as well as the orbital HST night. Such orbital and thermal changes cause an effect on the PSF known as breathing: the focus of the telescope changes slightly on short time-scales as the telescope truss responds to temperature changes in different parts of HST orbit (Hershey *et al.* 1998)

In order to reduce the scatter and noise, the photometric offset calculated from each image is averaged per epoch of observations and the standard deviation of the mean is provided. Figure 6 shows the resulting mean offsets at each WFC3/IR epoch *vs* time, with error bars indicating the standard deviation of the mean values at each averaged epoch. The linear fit of the offset over time is similar to that shown in Fig.4 with values of b = -0.0027±0.0004 at the 7σ level. Although the error bars are significantly reduced compared to the calculated individual offsets from each image, the resulting slopes are nearly identical.

To confirm that the IR sensitivity is linearly changing with time, the subset of well-measured stars were selected within the range of $-12.5 \lesssim$ Instrum.mag. $\lesssim -10$ and with the quality of fit parameter QU less than 0.05 (Fig.2). Then we recalculated the mean photometric offset like in Figure 4, but using only well-measured stars. Figure 7 shows that

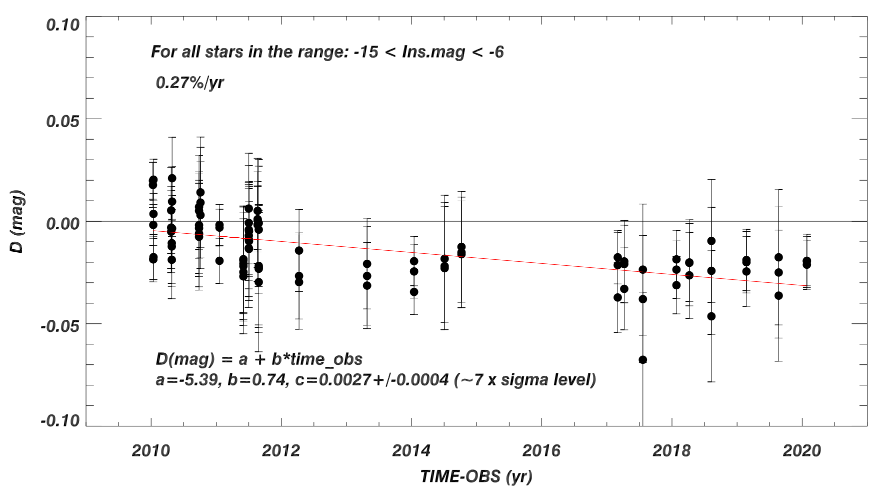

Fig. 4.— Average offsets calculated for all common stars in the magnitude range $-15 \lesssim$ Ins.mag. $\lesssim -6$, between the first (as reference image) and the next IR images as function of time. The over-plotted error bars are the calculated standard errors. The red solid line represents a linear fit to the averaged offsets as a function of time. The statistical coefficients and their errors are shown in the legend.

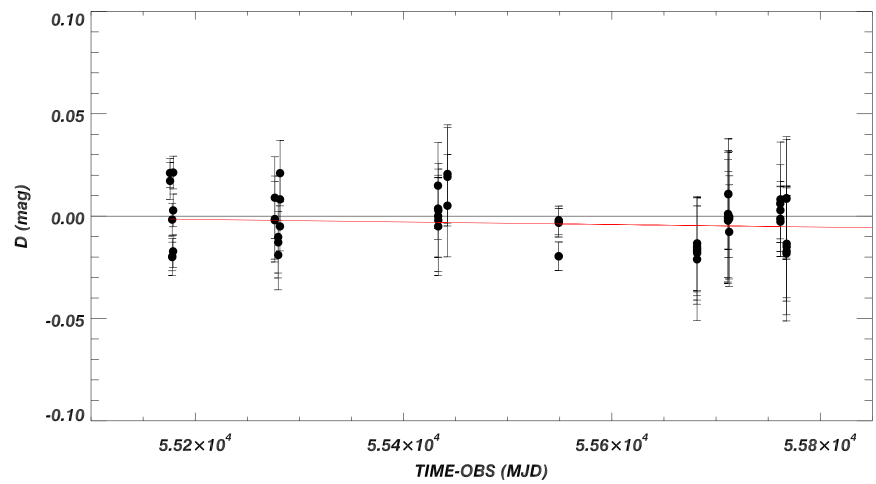

Fig. 5.— The same as figure 4, only for one year of observations *vs.* Modified Julian Date (MJD). The red line represents a linear fit of these photometric offset at that period of time

the IR sensitivity declines by $\sim 0.22\pm0.04\%$ per year but with much less scatter than the fit from all stars of individual images.

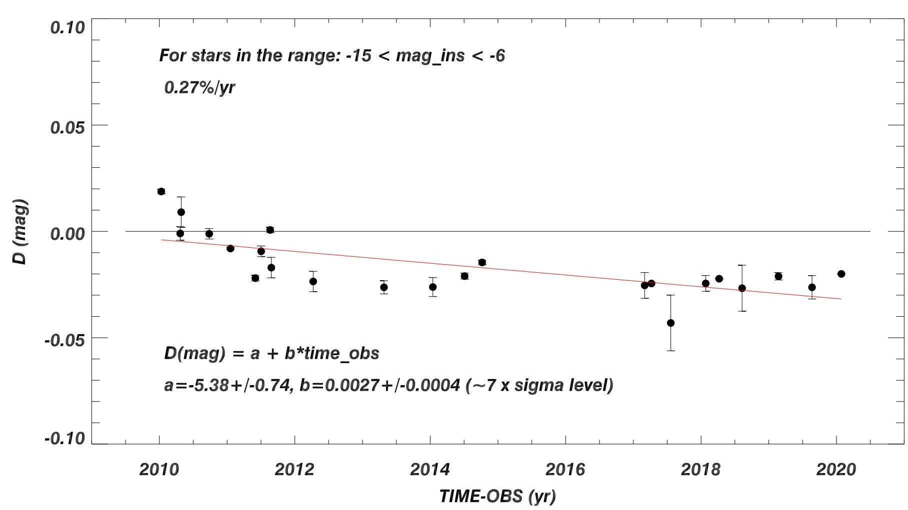

Fig. 6.— Same as figure 4, but using the average of individual offsets per each epoch and the error bars showing their standard deviation. Over-plotted red line shows the linear fit of mean offsets per epoch *vs.* time.

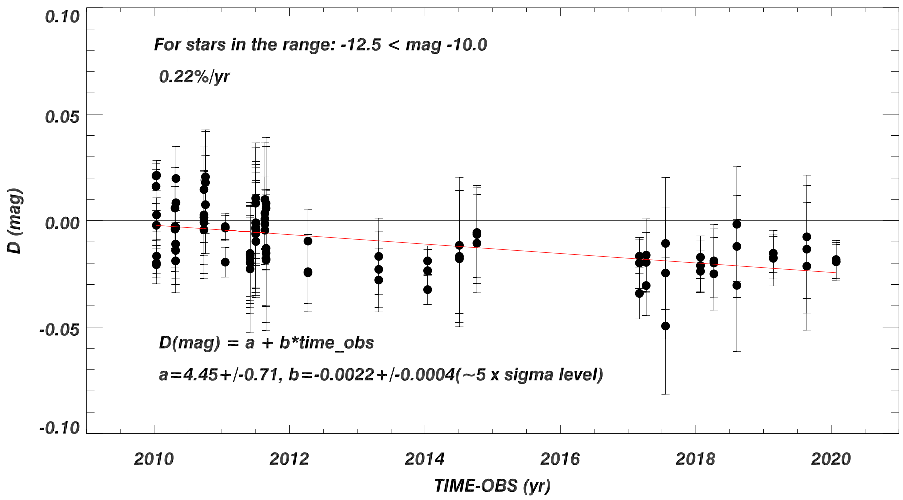

Fig. 7.— Photometric offsets calculated for well-measured stars. The over-plotted error bars are the calculated errors from each individual averaged photometric offset solution. The red solid line represents a linear fit of averaged offset *vs.* Time-Obs. The coefficients of the linear fit and its error are shown in the legend.

The self-persistence anomaly of the WFC3/IR detector generally seen in IR detectors, which can affect photometry at the level of 0.02-0.04 magnitudes (Long, K.S., *et al*, 2016). In order to minimize the effect of self-persistence of the WFC3/IR detector we performed the following test: the photometric offsets are calculated only from the first image obtained in each HST orbit from each astrometric calibration program for stars within the range of $-12.5 \lesssim$ Instrum.mag. $\lesssim -10$. Figure 8 shows the photometric offset as function of time for these selected observations. As can be seen from the figure, the WFC3/IR sensitivity is linearly decreasing over time by 0.25% per year, with a 3σ level of significance, rather lower than compare to all data were used.

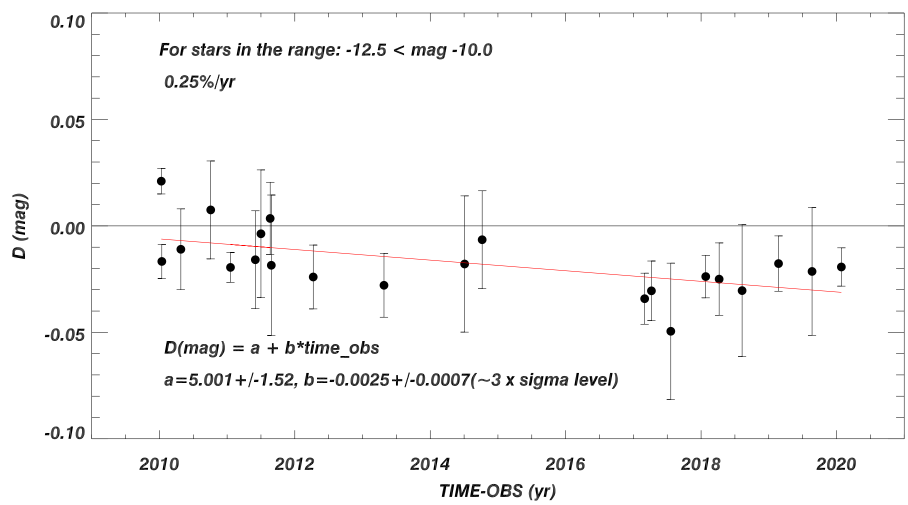

Fig. 8.— Photometric offsets calculated for well-measured stars from the first image on each HST orbit. The over-plotted error bars are the calculated errors from each individual averaged photometric offset solution. The red solid line represents a linear fit of averaged offset *vs.* Time-Obs. The coefficients of the linear fit and its errors are shown in the legend.

Figure 8 shows a significant scatter and hints of two possible separate distributions of the photometric offsets over two ranges of time: 2010 – 2012 and 2012 – 2020. In the first time range the character of the photometric offsets variations are uncertain. In the second range time, the photometric offset, in contrast to the first, appears relatively constant. We used two types of model for the photometric offsets at the first range time: 1) a linear function $f(D(mag)) = a + b \times T$ and 2) as a constant shift $f(D(mag)) = a$. In the second time range 2012–2020, we adopted a constant shift of the photometric offsets *i.e.* $f(D(mag)) = a$. As seen in Figure 9 there are two models in the range of time 2010-2012 presented by blue line as constant with a = -0.006±0.005 and the red line showing linear fit with the slope of coefficients b = -0.006±0.008. In both cases, the errors are effectively of the same order as the coefficient, it confirms that a simple offset model is more likely do be correct. For the second range of time the constant a = -0.025±0.003, and it is statistically significant at the $10\times\sigma$ level. Thus, the photometric offsets calculated from the first image on the HST orbit, excluding the exposure history from subsequent exposures have demonstrated that the WFC3/IR sensitivity is decreasing over time $\sim$ 0.2%/yr or there is the sensitivity drop of $\sim$ 0.2% in $\sim$ 2011.5. Such drop in sensitivity is substantial if the WFC3/IR high precision photometry is required between 2012 and the following observations.

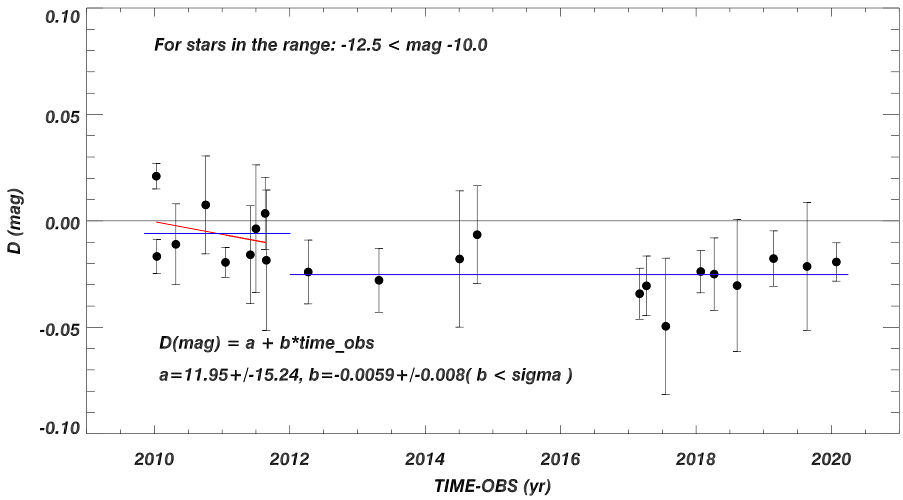

Fig. 9.— The same as Figure 8 only with three types of models, blue lines are constant for two periods of time. The red solid line represents a linear fit of averaged offset *vs.* time in the range of 2010-2012. The coefficients of the linear fit and its errors are shown in the legend.

4. Conclusions

The multi-cycle astrometric calibration programs of WFC3/IR observations of the globular cluster ω *Cen* have been used to examine the long-term trend in the IR throughput and its variation over time. Analysis of accurate ePSF fitting photometric results obtained from several thousand stars is used to calculate the photometric offsets over $\sim$11 yrs. Meticulous analysis of the calculated photometric offsets in the different magnitude ranges and the images taken at different time on orbit and different epochs shows consistent results that the sensitivity of WFC3/IR has has declined by ~ 0.2 % ± 0.04%/yr. However, we also were able to show that the loss of WFC3/IR sensitivity may not be a gradual change with time but could be consistent with a step-down in the sensitivity at 2011.5 and showing that before and after this event the sensitivity appears to me stable.

In addition to the long term changes of WFC3/IR sensitivity over time, there is also short term variation at the level of $\sim$ 2% in the timescale of a few HST orbits that is due to the well-known breathing effect, thermal changes on an orbital timescale.

In summary , we conclude that the changes in WFC3/IR sensitivity, are of the order of $\sim$ 0.2%/year, consistent with found by Bohlin & Deustua (2019) in the WFC3/IR grism data.

It is also important to note here that the changes are relatively small on the order of 0.002 magnitude per year and may not significantly affect the relative and/or absolute WFC3/IR photometry. However, the general observer must be aware that there is evidence for a a sensitivity loss in WFC3/IR detector and that should be taken into consideration when the WFC3/IR high precision photometry is required.

5. Acknowledgments

We express our gratitude to Jennifer Medina and Annalisa Calamida for reviewing this ISR and for all useful comments and suggestions which improved significantly the clarity of this ISR.

References

Anderson, J.,King, I., 2000, PASP, 112, 1360

Anderson, J., 2007, ACS Instrument Science Report, ACS-ISR-2007-08, (Baltimore:STScI)

Anderson, J., van der Marel, R.P., 2010, ApJ, 710,1032

Anderson, J., 2016, WFC3 Instrument Science Report, WFC3-ISR-2016-12, (Baltimore:STScI

Bajaj, V., 2019, WFC3 Instrument Science Report, WFC3-ISR-2019-07, (Baltimore:STScI)

Bohlin, R.C., Deustua, S.E., 2019, AJ, 157,229 ”CALSPEC:Wide Field Camera 3 Infrared Grism Spectrophotometry”

Dressel, L., *et al*, 2019, WFC3 Instrument Handbook, verion 12.0, (Baltimore :STScI)

Harris, W.E. 1996, AJ, 112, 1487

Hershey,J.,L., Eng. Team, 1998, “Document: SESD-97-01, version 2.0, 06-1998”

Kozhurina-Platais, V., Petro, L., 2012, WFC3 Instrument Science Report, WFC3-ISR-2012-03, (Baltimore:STScI)

Kozhurina-Platais, V., & Anderson, J., 2015, WFC3 Instrument Science Report, WFC3-ISR-2015-02, (Baltimore:STScI)

Long, K.,S., Baggett, S., M., Kozhurina-Platais, V., 2016, WFC3 Instrument Science Report, WFC3-ISR-2016-11, (Baltimore:STScI)